Large Eddy Simulation of Distillation Sieve Tray Hydrodynamics – A Volume-of-Fluid (VOF) Approach

A. Malvin, A. Chan, and P. L. Lau

Abstract—**A Large Eddy Simulation (LES) model is utilised to analyse the hydrodynamics of an industrial-scale distillation sieve tray. Three-dimensional two-phase flow of gas and liquid is considered in which the flow was modelled based on the concept of phasic volume defined in the Volume-of-Fluid (VOF) multiphase model. All governing equations including surface tension and wall adhesion are solved simultaneously using the commercial FLUENT code. The computational domain and operating conditions were adapted from experimental study where liquid velocity profiles, clear liquid height, and flow patterns were among the important quantities monitored. This work focuses on the improvement of the accuracy relative to experimental data with our new model over other existing Reynolds-Averaged Navier-Stokes (RANS) based models. Gas-liquid interfaces and the existence of froth regime are clearly visualised via the VOF model. The predicted quantities are found out to be in very good agreement with experimental data having discrepancies of less than 1.0%. Mesh resolutions above the bubbling area is identified as the key factor in accurate modelling of sieve tray hydrodynamics. The present model can be utilised with high confidence as the basis for the optimisation of sieve tray mechanical design.**

Index Terms—**Computational fluid dynamics (CFD), flow non-idealities, Large Eddy Simulation (LES), sieve tray, Volume-of-Fluid (VOF).**

I. Introduction

For the past decades, numerous works had been done to improve the efficiency of separation process in a tray distillation column. The majority, if not all, of these works were conducted in experimental manner aiming to correlate physical quantities observed under varying operating parameters. The outcomes were promising and as a result the design procedures of distillation column were formulated in the mostly practiced AIChE method summarized in the Bubble Tray Design Manual [1]. Despite the relatively low separation efficiency, most practitioners opt to rely on experiences to modify the tray design hoping to increase the underlying efficiency. However, as resources become more and more scarce and with the ever growing pressures from global communities to reduce carbon dioxide emissions, efficiency has again emerged as a prominent issue especially for this high energy demanding unit operation. To gain a better understanding on liquid flow pattern, thus better prediction on tray efficiency for a given tray configuration, it was inevitable to conduct either pilot scale or industrial scale experimental study. However, experimental works are practically laborious, time consuming and cost intensive. Depending on the scale of the system, experiment on tray column could sometime be hazardous.

Major improvement in computer technology, advancements in numerical methods and progression in multiphase flow models have allowed the use of computational fluid dynamics (CFD) technique in the study of intrinsically complex flow problems in distillation trays. Appreciable amount of computational studies, coupled by validation with reliable experimental data, have been conducted in the past ten years. Mehta *et al.* [2] simulated the liquid velocity distribution in an industrial-scale sieve tray by solving the liquid time-averaged equations of continuity of mass and momentum in a single phase steady-state three dimensional system. The presence of gas phase was, however, taken into account by introducing a liquid phase volume fraction term in the transport equation. The assumption of constant liquid volume fraction and the absence of vapour phase transport equation were identified as the main factors in the discrepancies from the experimental data. Yu *et al.* [3] developed a two-fluid two-dimensional flow model which introduces another set of transport equations to the dispersed vapour phase. This model rectified the deficiency found in the model proposed by [2]. Two-equation $k-\varepsilon$ turbulence model was utilized as the equations closure model. The resultant observation showed a good agreement with those published by [4] for outlet weir height of 50 mm. Severe discrepancies were, however, observed in the case when outlet weir height is 20 mm. This is due to the fact that at the near-wall, viscous force contributes to the formation of three-dimensional flow where the variation of velocity along the vertical direction is significant. Hence the prediction of two-dimensional theoretical model is invalid. Computational study on the effect of liquid loading, superficial gas velocity and weir height to clear liquid height was first attempted by [5]. The clear liquid height is defined by the height to which the aerated mass would collapse in the absence of vapour flow [6]. Volume-averaged mass and momentum conservation equations were solved in an Eulerian framework applying $k-\varepsilon$ turbulence model. A non-conventional rectangular tray and sieve holes were used in this simulation. Computational results obtained show a good agreement with correlation proposed by [7]. Deviations were, however, observed when compared to the experimental data and

Manuscript received December 20, 2010.

A. Malvin, A. Chan and P. L. Lau, Division of Environment, Faculty of Engineering, University of Nottingham Malaysia Campus, Jalan Broga, 43500 Semenyih, Selangor Darul Ehsan, Malaysia (phone: 603-8924-8622; fax: 603-8924-8017; e-mail: kebx8amv@ nottingham.edu.my).

correlation by [8]. These discrepancies were contributed by inadequate modelling of turbulence phenomena and the use of non-conventional design of tray and sieve holes. The use of rectangular holes geometry would influence the results associated with the use of Volume-of-Fluid (VOF) simulations for a priori prediction of bubble dynamics. Using the same turbulence and multiphase model, Van Baten and Krishna [9] simulated the tray hydrodynamics in a small-scale circular tray. Although tray hydraulics was well modelled, no attempt was made to validate the fluid flow patterns of industrial-scale sieve tray. Detailed works involving the use of two-fluid Eulerian-Eulerian framework were conducted by [10]. The extended downcomer region allows complete simulation of fluid flow behaviour in this region. Apart from this, liquid flow non-idealities namely stagnant zone, liquid recirculation and channelling were successfully modelled. Slight discrepancies on clear liquid height were observed when comparing with correlation by Bennett *et al.* [7]. The results obtained tend to overpredict the clear liquid height. However, [9, 10] agreed that these discrepancies were caused by the intrinsic limitation of the empirical correlations when dealing with froth regime.

The computational works conducted in the past decade share one similarity which is the use of $k-\varepsilon$ turbulence model as closure to the equation sets. The underlying reason is the relatively less expensive computational cost. However, the $k-\varepsilon$ turbulence model performs poorly in three dimensional flows and flows in the near wall region whereby the presence of shear is strong. Extensive works had been done by [11] to investigate the performances of different turbulence models mainly in the near-wall region. The results of the investigation concluded that no current Reynolds-averaged turbulence models (RANS) can predict the whole range of complex turbulent flows to worthwhile engineering accuracy. Although the Reynolds Stress Model (RSM) did appear to be superior to the Eddy Viscosity Model (EVM) and two-equation models, it is insufficient to warrant the abandonment of eddy-viscosity models.

The main objective of this work is to develop a computational model which is able to accurately predict the presence of flow non-idealities in a sieve tray. The proposed model is also able to rectify most of the discrepancies found in the previous computational works by incorporating the Large Eddy Simulation (LES) turbulence model as closure to equations sets and employing the VOF multiphase model which enable clear visualization of gas-liquid interfaces at any point in the system. The computational domain is generated based on the 1.213 m in diameter industrial-scale sieve tray used in experimental works by [12] involving an air-water binary system. Validation works will be based on comparison between computational results and published experimental data.

II. Computational Geometry

The computational domain models an industrial-scale sieve tray with diameter of 1.213 m as in [12]. Detail specifications of the sieve tray geometry are presented in Table I. Only half of the tray is modelled following observation of symmetric flow about the tray centre [12] to save computational cost and time. To allow full modelling of tray hydrodynamics, total numbers of 175 sieve holes are generated each with

Table I. Sieve tray specifications.

Description	*Dimension (m)*
Diameter, d_T	1.213
Hole diameter, d_H	0.0127
Weir height, h_w	0.05
Weir length, L_w	0.925
Tray Spacing, S	0.61
Clearance under downcomer, h_{cl}	0.038
% Bubbling area, A_B (over total area)	76%

diameter of 12.7 mm, arranged in a 0.05 m triangular pitch as shown in Fig. 1. The downcomer region is included to allow better representation of actual flow behaviour inside a tray column.

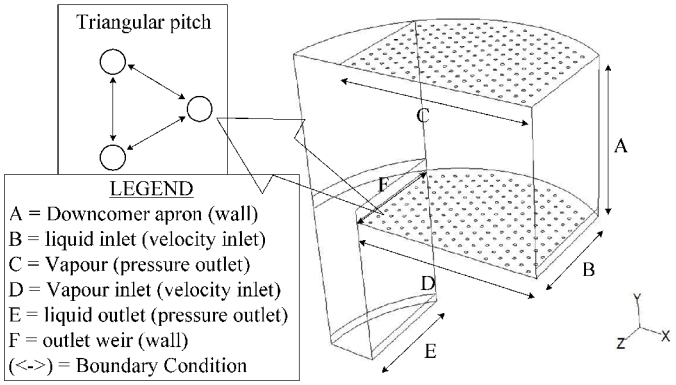

Fig. 1. Isometric view of computational geometry boundary conditions applied.

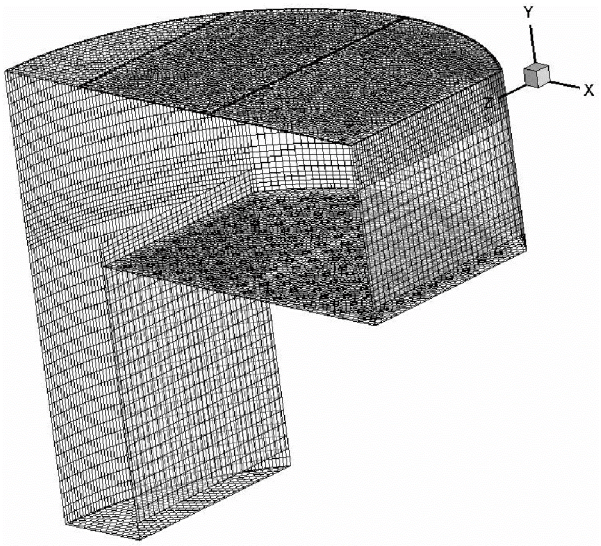

Fig 2. Mesh configurations of the computational domain.

The computational domain consists of hexahedral and polyhedral meshing elements. Mesh gradients were employed to the system with the active region (0m<y<0.038m) and the flow transition region (0.038m<y<0.3m) having interval sizes of 0.0095 m and

0.018 m respectively, as shown in Fig. 2. It is crucial to have sufficiently high mesh resolutions at these regions to attain accurate representation of gas-liquid interaction consequently the prevailing flow regime. Coarse meshes are applied to the remaining domain considering their minimum contributions to the system hydrodynamics. The number of computational cells generated ranges from 100,000 – 250,000 cells.

III. Governing Equations

In the proposed VOF multiphase model the tracking of gas-liquid interfaces is accomplished by the solution of a continuity equation for the volume fraction α of the two phases. Since the main focus of this work is on the hydrodynamic behaviour of sieve trays, energy transfers are not considered. Hence for the *qth* phase, the continuity equation is:

$$\frac{\partial \alpha_q \rho_q}{\partial t} + \left(\nabla \bullet \alpha_q \rho_q u\right) = 0 \ , \tag{1}$$

where u are the velocities. The fluid is considered incompressible and thus

$$\left(\nabla \bullet \alpha_q u\right) = 0 \ . \tag{2}$$

The volume fraction equation only solves for the secondary liquid phase whilst the primary gas phase volume fraction is computed based on

$$\sum_{q=1}^{n} \alpha_q = 1 \ . \tag{3}$$

The momentum equation is given by

$$\rho\left(\frac{\partial u_i}{\partial t} + u\left(\nabla \bullet u\right)\right) = -\nabla p + \mu \nabla^2 u + \rho g + F_{vol} \tag{4}$$

where p indicates pressure whilst g and F_{vol} represents gravitational acceleration and body force respectively. Continuum surface force (CSF) [13] is used to model the surface tension which is taken into account via the source term, F_{vol}, in the momentum equation. For two-phase flow, the volume force is defined by

$$F_{vol} = \sigma_{ij} \frac{\rho \kappa_i \nabla \alpha_i}{0.5\left(\rho_i + \rho_j\right)} \tag{5}$$

where subscript i and j denotes volume phases; σ represents the surface tension coefficient; κ represents the curvature defined by the divergence of the unit normal, $\hat{n}$

$$\kappa = \nabla \bullet \hat{n} \tag{6}$$

where

$$\hat{n} = \frac{n}{|n|} \tag{7}$$

in which

$$n = \nabla \alpha_q \tag{8}$$

Surface tension is determined by evaluating the Weber number, We which is given by

$$We = \frac{\sigma}{\rho_L L U^2} \tag{9}$$

where ρ_L represents liquid density; U represents the free-stream velocity and L represents the clearance under the downcomer. $We >> 1$ indicates that the presence of surface tension is significant and should not be neglected. In this work, given the air factor, F_s of 0.462, the calculated Weber number is approximately 7.3, indicating the strong influence of surface tension to the gas-liquid interface.

The governing equations of Large Eddy Simulation (LES) are obtained by filtering the time-dependent Navier-Stokes equations in the physical space. In the CFD code, the filtering operation is implicitly provided by the finite-volume discretisation. The filtered Navier-Stokes equations are:

$$\frac{\partial \alpha_q \overline{u}_i}{\partial x_i} = 0 \ , \tag{10}$$

$$\rho\left(\frac{\partial \overline{u}_j}{\partial t} + \overline{u}_i \frac{\partial \overline{u}_j}{\partial x_i}\right) = -\frac{\partial \overline{p}}{\partial x_j} + \mu \frac{\partial^2 \overline{u}_j}{\partial x_i^2} - \frac{\partial \tau_{ij}^r}{\partial x_i} + \rho g + F_{vol} \tag{11}$$

where $\overline{u}_i$ is the filtered resolved quantity in the ith direction; $\overline{p}$ represents the filtered pressure, and τ_{ij}^r is the residual stress tensor. Closure of the problems is achieved using the static Smagorinsky model [14]

$$\tau_{ij}^r = -2 v_t \overline{S}_{ij} \tag{12}$$

where $\overline{S_{ij}}$ represents the strain tensor given by:

$$\overline{S}_{ij} = \frac{1}{2}\left(\frac{\partial \overline{u_i}}{\partial x_j} + \frac{\partial \overline{u_j}}{\partial x_i}\right) \tag{13}$$

and v_t is the subgrid eddy viscosity given by:

$$v_t = l_S^2 S = \left(C_S \Delta\right)^2 S \tag{14}$$

where l_s is the Smagorinsky length scale; C_S is the Smagorinsky coefficient; Δ is the subgrid scale characteristic length and S is the strain-rate tensor given by $\sqrt{2}\left|S_{ij}\right|$. C_S value of 0.1 was adopted since at this point the Smagorinsky's model behaves reasonably well for free-shear flows and for channel flow [15]. All of the above governing equations, (1) – (14), are solved simultaneously using the commercial code FLUENT 6.3.

IV. Boundary Conditions

A. Liquid Inlet

As shown in Fig. 1, instead of mass flow inlet, velocity-inlet is specified as the liquid inlet boundary condition. Experimentally, tray-by-tray measurement of liquid mass flow rate entering from downcomer clearance is difficult to conduct and accuracy is always an issue. Most of the time, it is more convenient to express this quantity in term of liquid volumetric flow rate, Q_L, given by:

$$u_{L,in} = \frac{Q_L}{A_{da}} \tag{15}$$

The area under the downcomer apron, A_{da} is given by the product of downcomer clearance height, h_{cl} and weir length, l_w. In this work, only liquid is assumed to enter the system ($\alpha_L = 1$). This assumption is valid as the entrainment in this region is small and negligible [10]. In present work, only uniform flat liquid inlet profile was considered.

B. Gas Inlet

The velocity-inlet was specified as the gas inlet boundary condition. Direct measurement of gas velocity is often difficult to conduct experimentally, hence, a more convenient way is to express this quantity in term of superficial F-factor, often represented by F_S. This quantity is defined by the

product of gas superficial velocity, V_S and square root of gas phase density ρ_V as shown

$$F_S = V_S \sqrt{\rho_V} \quad . \tag{16}$$

Taking V_S as subject, equation (16) is then rearranged to

$$V_S = \frac{F_S}{\sqrt{\rho_V}} \quad . \tag{17}$$

For any given vapour load, the vapour superficial velocity can hence be calculated via (17). Having the bubbling area A_B as the basis of superficial velocity, the gas inlet velocity is then given by:

$$u_{h,i} = \left(\frac{V_S A_B}{2N_H} \right) \frac{1}{A_{h,i}} \tag{18}$$

N_H represents the number of sieve holes in the model geometry and $A_{h,i}$ stands for the hole area. The inlet gas volume fraction is assumed unity. Although entrainment always exists in the real industrial operation, its contribution towards the hydrodynamics of sieve tray is not significant.

C. Liquid and Gas Outlet

Pressure-outlet is specified as the liquid- and gas- outlet boundary conditions with backflow volume fraction of unity assigned at the secondary liquid-phase. This is to ensure that all of the down-coming liquid flows out via clearance under the downcomer apron. As such liquid and vapour flow across the tray are driven by the pressure gradient between the inlet and outlet of both entity.

D. Geometry Wall and Plane Symmetry

No-slip wall condition is specified to all wall boundaries. Wall adhesion is also modelled by specifying the contact angle between wall and liquid. A value of 90° is applied [16]. Planes indicating the centre of computational geometry were specified as symmetry boundary condition. At this plane, no flow and no scalar flux across the boundary occurs. Normal velocities are zero and the gradients of the other variables in the transverse coordinate direction are taken to be zero.

V. Operating Conditions and Solution Algorithms

The simulations were carried out at slightly above the atmospheric condition (114,600 Pa) with reference pressure location at x=0, y=0.5 and z=-0.305 [7]. Air and water are employed as the working fluids with air being specified as the primary gas phase whilst water being assigned as the secondary liquid phase. Since air is the dominant phase throughout the system, operating density was defined at 1.225 kg m^{-3} (density of the air).

The simulation is initialised by patching the liquid inlet surface with α_L =1 so that gas-liquid interfaces can be tracked immediately from the point of release. Apart from this, each time step is assumed to have fully converged whenever the continuity equation absolute criterion attained the value of 0.0001. This value is found to be adequate in assuring the convergence of the simulation based on the observation of liquid mass flow rate in the outlet stream and clear liquid height which are further discussed later. The most important factor which affects the convergence of the simulation is the time-step size Δt. In this work, the time-step size was evaluated based on the following relationship:

$$\Delta t = \frac{V_{cell,\min}^{1/3}}{U} \tag{19}$$

where $V_{cell,\min}$ is the minimum volume of the computational domain whilst U represents the fluids inlet velocity. With different values of air and water inlet velocity, the time-step size calculated varies from 0.005 s to 0.0001 s. However, better convergence was observed at Δt =0.0001 s.

Solution algorithms are introduced to enhance or accelerate the convergence of this simulation. The pressure velocity coupling is handled by the Semi-implicit Method for Pressure-linked Equation (SIMPLE) algorithm whilst Pressure Implicit with Splitting Operators (PRESTO) is used as the discretisation method. The solution algorithms are chosen based on trial-and-error procedures with the mentioned combinations result in the fastest convergence in term of computational time [17]. All of the simulations were conducted using 8 Intel Xeon processors 2.93 GHz run in parallels. Depending on the number of computational cells, computational time varies from 8 – 12 days.

VI. Results Analyses and Discussions

A. Convergence and Grid Independency Test

The transient simulation is deemed to have converged whenever the clear liquid height shows no considerable variation with time. At each time step, this variable is computed via the product of tray spacing and volume-average liquid phase volume fraction above the bubbling area of tray. As shown in Fig. 3, clear liquid height increased rapidly in the first 4s and gradually achieved steady-state after 8 s of computational flow-time. No significant variations are observed afterwards indicating the full convergence of computational flow-field. Sensitivity tests were therefore conducted by comparing the clear liquid height obtained from different grid sizes: 113,162 cells, 157,782 cells, 175,856 cells, 202,924 cells and 253,486 cells.

As shown in Fig. 4, clear liquid height varies significantly when grid sizes are less than 200,000 cells. Steady values are, however, observed at point beyond 200,000 cells. In spite of the precision offered at higher cell counts the use of ultra-fine meshes are avoided to reduce computational costs.

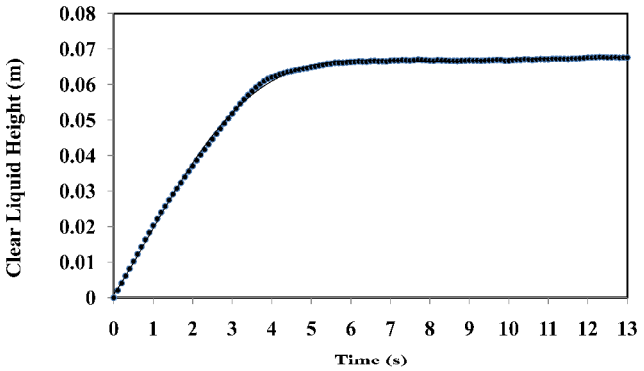

Fig. 3. Variation of clear liquid height as function of computational flow-time at Q_L = 17.8x10^{-3} m^3 s^{-1} and F_S = 0.462.

Since any increment beyond this point sees no significant changes in clear liquid height, grid size of 202,924 cells is hereby chosen as base model for the analysis of tray

hydrodynamics.

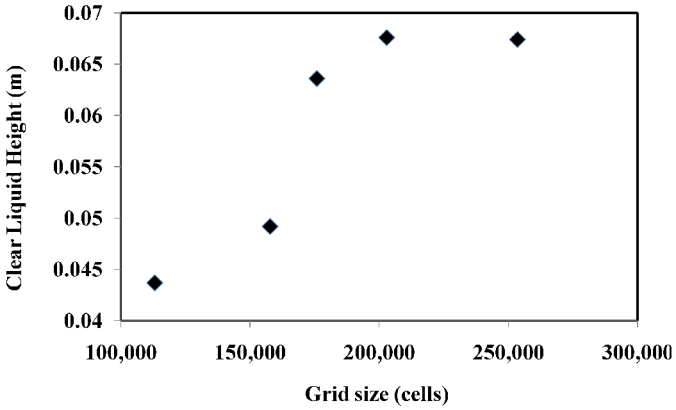

Fig. 4. Sensitivity of clear liquid height to grid resolutions.

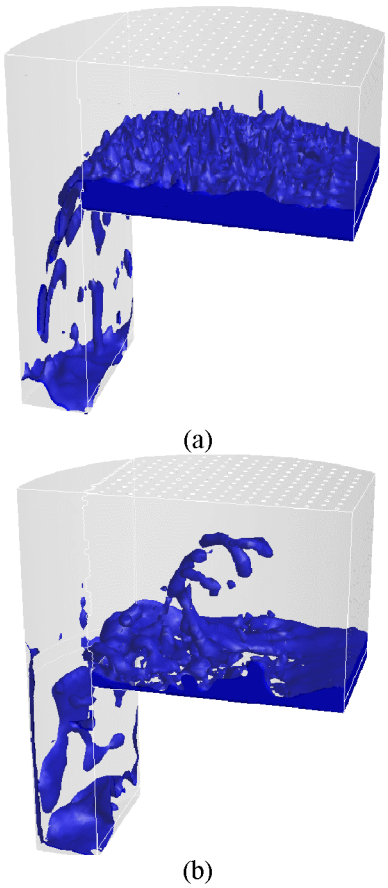

(a)

(b)

Fig. 5. Iso-surface visualization of liquid volume fraction at computational flow time, t = 13 s. (a) Mesh resolutions of 202,924 cells. (b) Mesh resolutions of 113,162 cells.

The effect of mesh resolutions can be readily observed via the iso-surface visualisation of liquid volume fraction. Two distinct observations are obtained despite the application of identical multiphase model. As a result of finer grid resolutions (more than 200,000 cells), Figure 5 (a) depicts better representation of air-water interaction. Water is evenly distributed across the tray with air coming up from the sieve holes for the purpose of mass transfer. The existence of froth regime, which is expected at the specified operating conditions, is also very well modelled.

On the contrary, coarser grid (less than 200,000 cells), as shown in Figure 5 (b), result in vast contribution of air flow in the tray centre which in turn directs the water flow to the near wall region. Instead of the presence of froth regime throughout the tray, localised frothing was observed in the region of tray centre creating false representation of tray hydrodynamics. Although the effect of different meshing elements cannot be readily observed via these figures, the smooth transitions between two interacting phases were postulated to be due to the structured polyhedral elements.

B. Clear Liquid Height

Validation of computational results is first carried out by comparing the calculated results with the published experimental data [12] and available correlations [7, 8]. As shown in Fig. 6, the proposed VOF-LES model shows remarkable accuracy and improvement, having maximum deviation of less than 1% from the experimental data.

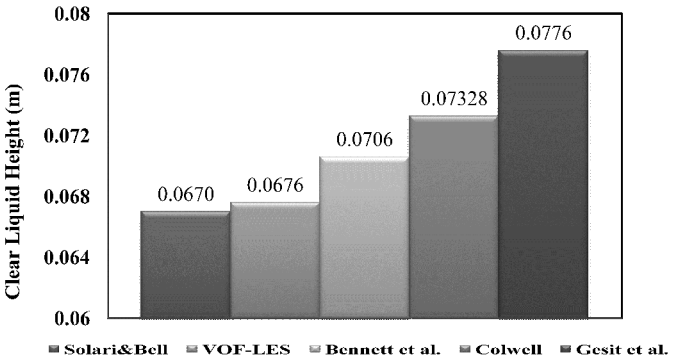

Fig. 6. Clear liquid height data at Q_L = 17.8x10^{-3} m^3 s^{-1} and F_S = 0.462.

Meanwhile, Colwell and Bennett correlations deviate approximately 5.4% and 9.4% respectively whilst Eulerian-Eulerian-$k-\varepsilon$ model proposed in [10] showing the largest discrepancy of 15.82%. The accuracy observed in VOF-LES model is due to the fact that all large-scale anisotropy motions (geometry dependent) are computed explicitly while only the smaller scales motions (which have a universal character) are being modelled by the subgrid eddy viscosity model.

Discrepancies in the Colwell and Bennett correlations are attributed to the intrinsic limitation of the empirical correlations when dealing with froth regime. The constants associated with the use of these correlations are often defined for a specific system. In other words, one has to conduct an experiment in a scale identical to the studied system in order to obtain accurate constant values. However, in the economics and safety point of view, this is often difficult, if not impossible, to conduct owing to the size and inherent hazards of the systems. In addition, the difference in geometric scale may also contribute to the discrepancies observed. Bennett et al. [7] utilised a 0.6 m sieve tray with sieve holes diameter of 3 mm, in contrast to the system modelled in the present work which is twice the size.

Meanwhile, Gesit *et al.* [10] pointed out that the discrepancies in the proposed Eulerian-Eulerian - $k-\varepsilon$ model are contributed by the insufficient spatial resolution of the flow near the tray floor and the use of smaller number of sieve holes which leads to channeling, consequently an increased in clear liquid height. However, it must be noted that the choice of turbulence model plays significant role in the accurate representation of flow phenomena prevailing

inside the tray. Owing to the fact that the $k-\varepsilon$ turbulence model performs poorly in the system where the presence of shear is strong, it can be concluded that the choice of turbulence model is the main factor contributing to the major discrepancy in [10].

C. *Upstream and Downstream Liquid Velocity Profiles*

Further validation work was carried out by comparison of liquid velocity profiles with the experimental data. As shown in Fig. 7, Solari & Bell [12] in their experimental study installed measuring probes at elevation of 0.038 m above the tray floor. These probes were used to obtain liquid velocity magnitude at corresponding points. Region bounded by x = -0.046 and x = 0.183 represents the upstream region whilst region bounded by x = -0.275 and x = -0.046 represents the downstream region. Liquid velocity magnitude was averaged along the x-axis as function of z-axis.

Unlike time-averaging method utilised in the RANS model, LES allows the evaluation of instantaneous velocity profiles across the tray. Velocity magnitude data can therefore be obtained at any point of time allowing close resemblance in terms of data sampling method used in the experimental work by [12]. Both upstream and downstream liquid velocity profiles are evaluated at computational flow-time = 13 s in which steady-state was observed, as shown in Fig. 3.

It can be seen, from Fig. 8 and Fig. 9, that highest velocity magnitude exists in the region of tray centre. The magnitude then decreases gradually as it moves along the z-axis towards the column wall indicating the presence of non-uniform velocity distribution. Stagnant zone, represented by velocity magnitude of less than 0.1 m s^{-1}, can be clearly observed in the near-wall region (z/R~1). These observations are in good agreement with the experimental finding by [12].

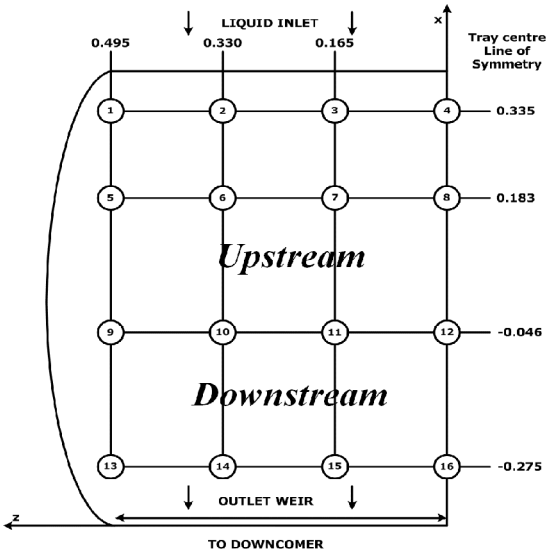

Fig. 7. Measuring probes position in the experimental work by Solari and Bell [12]. The diagram depicts half tray geometry in the absence of calming zone.

Meanwhile, fluctuations in liquid velocity magnitudes are due to the contribution of upward gas phase momentum created by the injection of air via the sieve holes. In contrast to the Eulerian-Eulerian multiphase model, in VOF, fluids of different phases are not interpenetrating and that a single set of momentum equations is shared by the fluids. In other words, the velocity magnitude shown in Fig. 8 and Fig. 9 signify the mixture phase instead of individual liquid phase. In spite of the fluctuating parts, the overall trends correspond reasonably well with both [10] and [12].

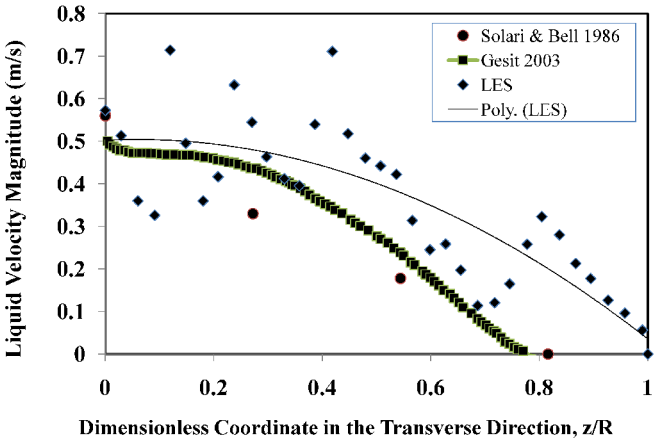

Fig. 8. Upstream liquid velocity profile at Q_L =17.8x10^{-3} m^3 s^{-1} and F_S = 0.462.

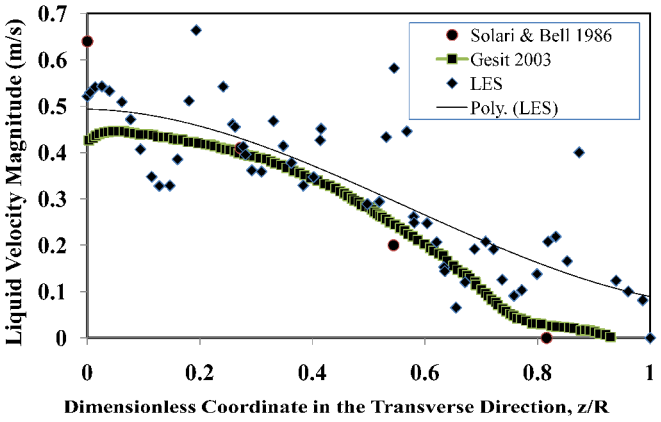

Fig. 9. Downstream liquid velocity profile at Q_L =17.8x10^{-3} m^3 s^{-1} and F_S = 0.462.

D. *Flow non-idealities*

In order to gain an insight into the gas-liquid flow behaviour in a sieve tray, it is useful to observe the velocity magnitude vector plot as shown in Figure 10. Liquid entering from the inlet downcomer channelled through the tray centre seeking for the shortest path to the outlet weir and leaving stagnant zone near the column wall region. Region beneath the red line depicts the presence of liquid channelling whilst the above region depicts the presence of stagnant zone. Stagnant zone is defined by the region in which liquid velocity magnitude is less than 10% of its highest magnitude i.e. u_L < 0.2 m s^{-1}. In Fig. 10, this region is marked by the dark blue vectors.

Unlike experimental study, the present model is able to quantify the degree of liquid stagnation via region segregation method. Volume of liquid above the tray is first quantified based on the computed clear liquid height followed by segregation of liquid volume with velocity

magnitude of less than the specified cut off value of 0.2 m/s.

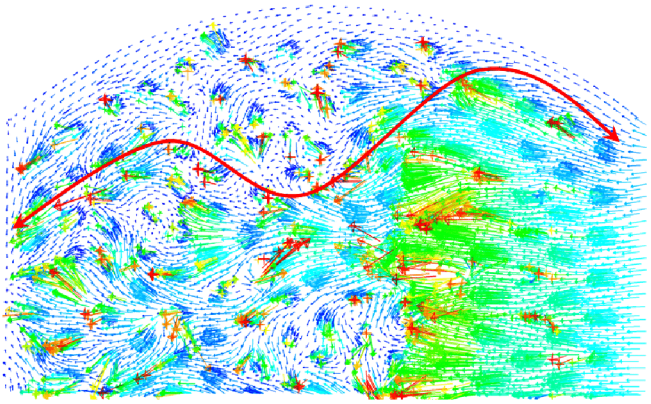

Fig. 10. Vector of liquid velocity magnitude at elevation of y = 0.038 m, at computational flow time of t = 13 s.

It is found out that 21.66% of the liquid above the tray is in the stagnation condition. In the other words, only 78% of the liquid is exposed to proper mass transfer.This finding further explicates the poor separation efficiency often observed in industrial practice. Although the presence of air flow has significantly reduced the presence of recirculation zones by creating more turbulent in the near wall region [3, 12], it is still inadequate to fully eliminate the presence of stagnant zone. In overall, the prevailing flow non-idealities are in very good agreement with experimental observations by [6, 10, 12].

VII. Conclusion

The present work attempts to model the hydrodynamics of industrial-scale sieve tray using VOF-LES model. The flow behaviour in distillation tray was modelled as three dimensional two-phase flows of gas and liquid. The governing equations, (1)-(14), are solved using the FLUENT code. Computational results are validated by means of comparison of quantities such as clear-liquid height and liquid velocity profiles with published experimental results [12] and available correlations [7, 8]. In overall, the computational results show very good agreement with experimental data.

Massive efforts and resources have been spent in the past decades to understand the complex flow behaviour prevailing in the distillation sieve tray. However, till present, having so many published correlations, uncertainties still exist in the design of sieve tray. This work has, however, proven that CFD method is able to answer those uncertainties effectively. Clear liquid height was computed with remarkable accuracy and the prevailing flow regime was predicted very well for this given operating conditions. In conclusion, the proposed VOF-LES model has successfully modelled the hydrodynamics of distillation sieve tray and thus can be utilized with high confidence in the optimization of tray design.

References

[1] AIChE, *Bubble Tray Design Manual, New York: American Institute of Chemical Engineers*. New York: American Institute of Chemical Engineers, 1958.

[2] B. Mehta, K. T. Chuang, and K. Nandakumar, "Model for liquid phase flow on sieve tray," *Chemical Engineering Research and Design,* vol. 76, pp. 843-848, 1998.

[3] K. T. Yu, X. G. Yuan, X. Y. You, and C. J. Liu, "Computational fluid-dynamics and experimental verification of two-phase two-dimensional flow on a sieve column tray," *Chemical Engineering Research and Design,* vol. 77a, pp. 554-560, 1999.

[4] K. E. Porter, K. T. Yu, S. Chambers, and M. Q. Zhang, "Flow Patterns and Temperature Profiles on a 2.44 m Diameter Sieve Tray," *Transaction of Institute of Chemical Engineering (Trans IChemE),* vol. 70a, pp. 489-500, 1992.

[5] R. Krishna, J. M. van Baten, J. Ellenberger, A. P. Higler, and R. Taylor, "CFD Simulations of Sieve Tray Hydrodynamics," *Transaction of Institute of Chemical Engineering (Trans IChemE),* vol. 77(a), pp. 639-646, 1999.

[6] H. Z. Kister, *Distillation Design*. New York: McGraw Hill, 1992.

[7] D. L. Bennett, R. Agrawal, and P. J. Cook, "New Pressure Drop Correlation for Sieve Tray Distillation Columns," *AIChE Journal,* vol. 29, pp. 434-442, 1983.

[8] C. J. Colwell, "Clear Liquid Height and Froth Density on Sieve Trays," *AIChE Journal,* vol. 20, pp. 298-307, 1981.

[9] J. M. van Baten and R. Krishna, "Modelling sieve tray hydraulics using computational fluid dynamics," *Chemical Engineering Journal,* vol. 77, pp. 143-151, 2000.

[10] G. Gesit, K. Nandakumar, and K. T. Chuang, "CFD modelling of flow patterns and hydraulics of commercial-scale sieve trays," *AIChE Journal,* vol. 49, pp. 910-924, 2003.

[11] P. Bradshaw, B. E. Launder, and J. L. Lumley, "Collaborative Testing of Turbulence Models (Data Bank Contribution)," *Journal of Fluid Engineering,* vol. 118, pp. 143-247, 1996.

[12] R. B. Solari and R. L. Bell, "Fluid Flow Patterns and Velocity Distribution on Commercial–Scale Sieve Trays," *AIChE Journal,* vol. 32, pp. 640-649, 1986.

[13] J. U. Brackbill, D. B. Kothe, and C. Zemach, "A continuum method for modelling surface tension," *Journal of Computational Physics,* vol. 100, pp. 335-354, 1992.

[14] J. Smagorinsky, "General Circulation Experiments with the Primitive Equations, I. The Basic Experiment," *Monthly Weather Review,* vol. 19, pp. 99-164, 1963.

[15] O. C. Zienkiewicz, R. L. Taylor, and P. Nithiarasu, *The Finite Element Method for Fluid Dynamics*, 6th ed. Oxford: Elsevier Butterworth-Heinemann, 2005.

[16] FLUENT, "FLUENT 6.3 User's Manual," FLUENT Inc., 2006.

[17] A. Malvin, A. Chan, and P. L. Lau, Large Eddy Simulation of Distillation Sieve Tray Hydrodynamics using Volume-of-Fluid (VOF) Multiphase Model, *Lecture Notes in Engineering and Computer Science: Proceedings of The World Congress on Engineering and Computer Science 2010, WCECS 2010, 20-22 October, 2010,* San Francisco, USA, 2010, pp. 800-805.